AMUSE Asteroid Simulations

Tünde Meijer, Kutay Nazli, Claire Olde Loohuis

November 2022

Abstract

Context. The Yarkovsky–O'Keefe–Radzievskii–Paddack (YORP) effect is the total torque induced on small asteroids caused by the anistropic reflection of the sunlight due to surface or albedo irregularities and the force caused by the thermal re-emission of photons absorbed by the asteroid. It can most easily be observed in the light curves of small near-Earth asteroids (NEAs).
Aims. To create accurate in-situ simulations of asteroids with varying surface parameters under the torque induced by YORP effect and produce and compare light curves of these asteroids with ones where YORP effect is neglected.
Methods. This work builds onto the existing AMUSE framework which it uses to build and calculate n-body gravitational simulations and stellar parameters. Asteroids are treated as simple spheres with constant surface parameters to build a toolkit to calculate directions of the light source and the observer, and subsequently determine illuminated faces. Then, asteroids are modeled as spheres with tessellated surfaces to model the added effects of the YORP torques. Finally, light curves are created at the observer location through flux calculations over the tessellated surface.
Results. We successfully implement the YORP and Yarkovsky effects on a spherical near-Earth asteroid in an AMUSE framework, and are able to calculate the flux from the asteroid as seen by an observer anywhere in the solar system. Various methods of generalization and next steps for the project are discussed.
Conclusions. Though the YORP and Yarkovsky effects are not always visible on small timescales, we find that they have a marked effect on large timescales both in terms of asteroid precession and orbital parameters, and that the observed parameters of the asteroid show this. We find additionally that in principle we are able to extend our calculations to non-spherical, though still convex, asteroid shapes.

1 Introduction

The Yarkovsky-O'Keefe-Radzievskii-Paddack (YORP) effect, or commonly known as the non-gravitational effect, describes the total torque induced on small asteroids caused by the Solar radiation incident on the object. It is generally split into two components: the anistropic reflection of the sunlight due to surface or albedo irregularities (rotational variant or the YORP effect) and the force caused by the thermal re-emission of photons absorbed by the asteroid (thermal variant or Yarkovsky effect). Since it was coined by Rubincam (2000), it has been extensively studied and identified as one of the important mechanisms that guide the physical and dynamical evolution of the asteroid population.

It has been theorized that the combined effect of the two forces can accelerate asteroids to the rotation break limit, cause them to shed mass, or create pairs or binaries of asteroids in the small scales. In the larger scales, it helps shape the rotation rate and obliquity distribution of the asteroid population. The details of the theoretical backgrounds of these effects and the relevant references can be found in the review of Vokrouhlický et al. (2015).

As of the writing, there has been ten observationally detected cases of the YORP effect, all on small-sized near-Earth asteroids (NEAs). This observational selection bias is mainly due to the inverse square dependence of the YORP torque on the distance from the light-source via the incident flux, and on the radius of the asteroid via the mass-to-radius ratio. These asteroids are: (54509) YORP (Lowry et al., 2007; Taylor et al., 2007), (1862) Apollo (Kaasalainen et al., 2007; Ďurech et al., 2008), (1620) Geographos (Durech et al., 2008; Ďurech et al., 2022), (3103) Eger (Ďurech et al., 2012, 2018), (25143) Itokawa (Lowry et al., 2014; Ďurech et al., 2008), (161989) Cacus (Ďurech et al., 2018), (101955) Bennu (Nolan et al., 2019; Hergenrother et al., 2019), (68346) 2001 KZ66 (Zegmott et al., 2021), (1685) Toro (Ďurech et al., 2018, 2022), and (10115) 1992 SK (Ďurech et al., 2022). Of interest is the fact that all of these observations are of accelerating rotations, even though both theory (Rubincam, 2000) and best-fitting simulations of observational asteroid population parameters (Rossi et al., 2009) do expect cases of deceleration as well.

Most of the modern research into the orbital/physical parameter and shapes of asteroids with observed YORP-related accelerations (Tian et al. (2022) and as discussed above) use light-curve inversion methods developed by Kaasalainen and Torppa (2001); Kaasalainen et al. (2001). Even though the shape results have been tested on ray-traced stationary asteroids and the observational parameter models have been tested on well-observed asteroids, simulations of asteroids with complex shapes and surface parameters in their natural environments have yet not been done.

Even though this work mostly focuses on discussing NEAs and the effect of the YORP torque, this framework can be generalized to many other areas. Some interesting recent studies include calculating the YORP force for defunct satellites in geosynchronous orbit for predictive priority in debris removal and servicing mission (Benson and Scheeres, 2021) or calculating the orbit decay of planetary remnants around white dwarves due to reduced Yarkovsky forces (Veras et al., 2022). Accurate calculations and simulations of asteroid orbits is also of utmost importance for asteroid landing, redirection and other Earth-defense missions such as NASA's Double Asteroid Redirection Test (DART) and its descendants where torques induced by YORP is vital to the trajectory determination (Naidu et al., 2022).

Looking at the field as a whole, modern work in studying the YORP effect relies heavily on post-observational modelling and parameter fitting, and mostly assuming a linear change of momentum due to the torques. Even though extensive archival observations of these asteroids exist, the observational sample size remains small, which constrains the development of parameter-fitting tools and thus the extent to which the theory can be validated. This work aims to supplement existing AMUSE simulation framework with a starting point for accurate, in-situ simulations of asteroid motion in the Solar system which can be extended to other stellar systems/objects and to forces with surface property or shape dependency. This capability would allow for better understanding of both the case-by-case effects such as the lack of deceleration observations, or the population-wide effects such as binary formation or time-evolution of rotation rate distributions. It would also allow for better integration of the YORP force and testing of the light-curve inversion methodology by providing extensive synthetic observations of asteroids with known parameters.

2 Methods

2.1 Theoretical Background

The infinitesimal force $d\mathbf{f}_{\text{sca}}$ caused by the scattering of photons of an infinitesimal surface $d\mathbf{S}$ is given by:

$$d\mathbf{f}_{\text{sca}} = -\frac{F}{c}(K_1^{\text{sca}}\mathbf{n}_\perp + K_2^{\text{sca}}\mathbf{m})dS \tag{1}$$

where F is the incident flux, c is the speed of light, K_i^{sca} are the components of the surface scattering function in directions $\mathbf{n}_\perp$ of the surface normal and $\mathbf{m}$ in the horizon plane of $d\mathbf{S}$ defined by:

$$\mathbf{m} = \frac{\mathbf{n}_0 - \mu_0\mathbf{n}_\perp}{\sqrt{1-\mu_0^2}}$$

where $\mathbf{n}_0$ is the unit vector in the direction of the Sun and $\mu_0 = \mathbf{n}_\perp \cdot \mathbf{n}_0$. Similarly, the thermal re-emission force is given by

$$d\mathbf{f}_{\text{th}} = -\frac{\sigma T^4}{c}(K_1^{\text{th}}\mathbf{n}_\perp + K_2^{\text{th}}\mathbf{m})dS \tag{2}$$

where σ is the Stefan–Boltzmann constant, T is the surface temperature and K_i^{th} are the thermal counterparts of the surface scattering function.

In the simplest solution that will be adopted in this work, using Lambert's law to model scattering and thermal emission, one gets:

$$K_1^{\text{sca}}(\mu_0) = \frac{2}{3}\mu_0 A \qquad K_2^{\text{sca}}(\mu_0) = 0$$

$$K_1^{\text{th}}(\mu_0) = \frac{2}{3}\epsilon \qquad K_2^{\text{th}}(\mu_0) = 0$$

where A is the surface albedo and ϵ the characteristic emissivity constant. This assumption reduces the forces to

$$d\mathbf{f}_{\text{sca}} = -\frac{2}{3}\frac{\mu_0 A F}{c}\mathbf{n}_\perp dS \tag{3}$$

$$d\mathbf{f}_{\text{th}} = -\frac{2}{3}\frac{\epsilon\sigma T^4}{c}\mathbf{n}_\perp dS \tag{4}$$

which, given a simple surface where properties are assumed to be constant over, can be easily integrated to the full forces with a surface integral.

Finally, though most of the properties discussed above can be assumed to be constant during the time evolution of the simulation, the temperature T is highly dependent on the surface flux and therefore cannot be assumed to be intrinsic to the surface of the asteroid. However, it can be calculated using the conservation of energy equation for the asteroid infinitesimal surface

$$\epsilon(\mu_0)\sigma T^4 + K\mathbf{n}_\perp \cdot \nabla T = (1 - A_h(\mu_0))\mu_0 F \tag{5}$$

where $A_h(\mu_0)$ is the hemispherical albedo. Under the Lambert approximation and the additional Rubincam approximation which assumes $K = 0$, one can reduce this equation to simply $\epsilon\sigma T^4 = (1 - A)\mu_0 F$ which allows for direct derivation of the temperature from the incident flux and other surface parameters.

2.2 Simulations

The simulations for this work consist of evolving primarily three forces in a system mimicking the Solar system: the gravitational attractions between Solar system objects and the asteroid(s) in an n-body simulation and the added effects of the thermal and rotational forces on the asteroids. The n-body gravitational code used is Hermite provided by the AMUSE framework, while code that handles the calculations of the YORP and Yarkovsky forces is developed specifically for this work. The trajectories of the individual bodies are therefore determined by integrating these forces iteratively in time using a bridge, which is native to AMUSE. A visualization of the bridge setup is in Figure 1.

For the base-level simulations, as aforementioned, the system is made to mimic the Solar system, however a *Python*-class that initializes desired systems from a .json file with predetermined structure is also built to facilitate the generalizability of the framework. This class, called the *System*-class, is also used to house the various *amuse.lab.Particles* objects used to simulate the Solar system objects apart from the asteroids, as well as designating the observer and observables, calculating the directions to the Sun and the observer from an observable and calculating forces and fluxes. It should be noted that all bodies in the simulation are treated as point masses, and that

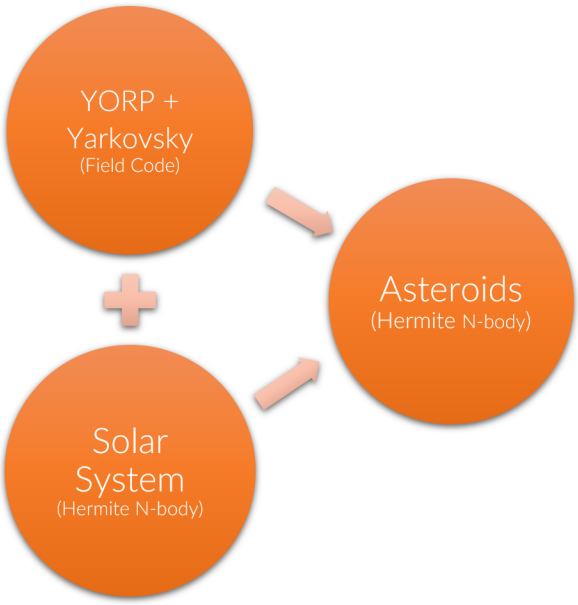

Figure 1: AMUSE bridge setup. The asteroid n-body is perturbed by the Solar system gravity as well as the YORP/Yarkovsky field code. The Solar system n-body has no perturbers, as neither the gravitational effects of the asteroids nor the effect of the field code is strong enough to modify orbits on a planetary scale.

stellar evolution is not taken into account; it is not expected for the incoming Solar flux on the asteroids to change significantly over the integration time of simulations presented in this work.

Specifically within this system, the asteroids are created as a special subclass of the *amuse.lab.Particle* class with added functionality. In addition to the methods available in AMUSE, the *Asteroid*-class has access to its own surface tessellations and methods to calculate YORP and Yarkovsky forces and outgoing flux for itself.

In more detail, the asteroids in this simulation are created as spheres with surface patches or tessellations that are shaped like distorted squares

generated through surface mapping a uniformly tessellated cubic surface onto a spherical surface. This method was chosen for its simplicity of creating smaller flat surfaces on the surface on a spherical object with near-equal (and analytically calculable) surface area over which the Lambert and Rubincam assumptions can be used. This also creates a very robust basis for creating more complicated surface shapes by either morphing or joining the resultant tessellated spheres, or by simply using other cube-to-surface mappings analytically calculable.

With these tessellations as a basis, the resultant YORP and Yarkovsky torques on the asteroid can be calculated by the sum of the surface integrals over the small patches, as all of the patches have their own physical surface properties (albedo, ϵ, area etc.), and their spatial properties ($\mathbf{n}_\perp, \mathbf{n}_0$ etc.) can easily be calculated in every time-step of the simulation. The same can also be said for the flux calculation. Using the $\mathbf{n}_\perp$ and $\mathbf{n}_0$ directions allows for determination whether a given surface is illuminated or not, and adding the capability of the *System*-class to calculate the direction to the observer allows for the determination of whether it is visible. If a given surface is both illuminated and visible, its flux can be transferred to the total flux calculation depending on whether it is reflecting or re-emitting. This allows for the calculation of the light-curves, which is one of the desired results of these simulations.

A detailed description of what is discussed in this section and of the code developed can be found in a code overview document on our GitHub.

As a final note, this work only considers convex geometries for asteroids, which is by no means a generalizable assumption. The question of self or object-to-object shadowing is important when considering concave geometries or dense asteroid populations, and even though this work does not consider these cases, it allows for framework to be built upon what is developed with ease to implement these determinations. Kaasalainen and Torppa (2001) discusses these methodologies in detail, but simply put, it is possible to determine if a given surface shadows another given $\mathbf{n}_\perp$, the center of the patch and $\mathbf{n}_0$ through either an N^2 or $\mathrm{N} \log \mathrm{N}$ process to first order (excluding partial occultation).

2.3 Initial Conditions

Though the structure of the code allows for near-endless variation, for this work we endeavored to make the simulation as simple as possible while remaining as accurate as possible. Initial conditions are listed in Table 1.

Asteroid mass	470 kg
Asteroid radius	0.3 km
Asteroid semi-major axis	1.126 AU
Asteroid albedo	$\sim \mathcal{U}_{[0,1]}$
Asteroid emissivity	0.65
Orbital phase Earth	$\pi/4$
Orbital phase Jupiter	$\pi/6$
Orbital phase asteroid	$-\pi/4$
Observer size	$2000R_{\oplus}$
Simulation timestep	0.01 year
Simulation end-time	10 years

Table 1: Initial conditions for simulations. All unlisted parameters of the Solar bodies are accurate to best known values, with the added assumption of coplanarity and circular orbits. The unlisted asteroid values are variables of interest.

The simulated Solar system includes bodies which have the largest gravitational effect on the asteroid: the Sun, the Earth, and Jupiter. The incorporation of Jupiter is due to its marked resonance effect on Solar system asteroids, as expressed in Burns and Hamilton (1992). The Earth has been assigned as the point of residence for the observer, though in principle any planet could be designated as such. All planet parameters are true to accepted values, except the orbits are assumed to be circular and coplanar.

Parameters of the asteroid, including its radius, semi-major axis and emissivity were chosen to represent those of a common Near-Earth asteroid (NEA). To make the orbital changes resulting from YORP/Yarkovsky forces observable on smaller time scales, the mass of the asteroid was scaled down significantly. While an NEA of this size is expected to have mass of around 10^10 kg, the simulated asteroid was given a much smaller mass of 470 kg,

resulting in a roughly 8-orders of magnitude increase in resulting acceleration, making the orbital changes (and subsequently changes in the flux curves), much more tangible. The individual patches on the asteroids were taken to be roughly $\sim$ 30m in size to match the surface irregularities seen of NEAs in direct optical observations. These tesellated patches were given random albedos $\sim \mathcal{U}_{[0,1]}$ to mimic the differing bright and dark patches due to material differences and more importantly surface features on asteroids.

One final parameter of interest is the size of the observer. It is chosen to be unrealistically large ($2000R_{\oplus}$) to combat the overly precise nature of the naive ray tracing implemented in the simulations. This is due to two factors: 1) the rays are traced from the source (the Sun) to the observer, and 2) the observer is a point. Since only principle rays per surface patch are traced from the source to the point-like observer, the likelihood of a ray bouncing off of an asteroid surface patch being received is infinitesimal. This can be corrected via tracing more than the principle ray, but this linearly increases calculation time per surface patch. Even so, the odds would remain infinitesimal due to the size of the observer. While the ideal and expensive solution would be to trace the multiple rays from the point-like observer back to the source, an easier solution that does not introduce a linear scaling to the runtime would be to increase the size of the observer to compensate, which is implemented here.

3 Results

The plot displaying the positions of the asteroid throughout the simulation with a timescale of 10 years and a time step of 0.01 years, can be seen in Figure 2. The Sun is displayed at the center in orange, the blue line denotes the orbit of the Earth, and the gray shows the orbit of the asteroid over time. Arrows attached to the orbit of the asteroid show the combined magnitude and direction of the YORP/Yarkovsky forces. Though the orbit of Jupiter is not shown in this plot, its effects are still taken into account in the simulation.

Figure 3 displays the positions of an asteroid that isn't affected by the YORP/Yarkovsky effect, and Figure 4 shows the semimajor axis and eccentricity for both cases. Comparison with an asteroid affected shows that indeed the simulated extra acceleration due to the YORP/Yarkovsky forces causes

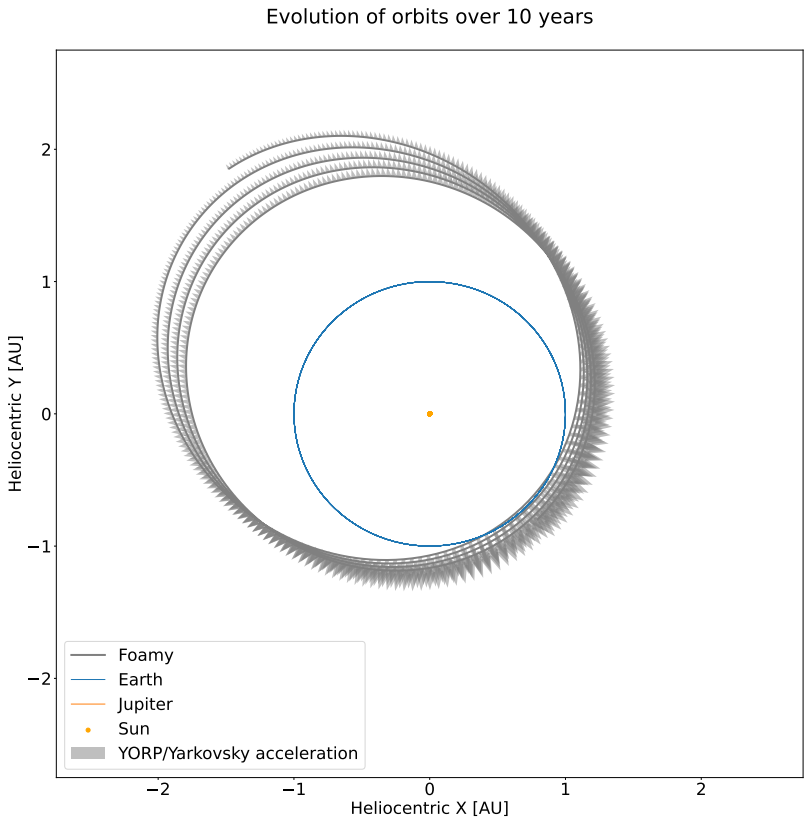

Figure 2: The evolution of the orbit of an asteroid with initial conditions as listed in Table 1.

the orbit of the asteroid to decircularize via pushing the asteroid radially outward. The particular shape of the orbit depends on two factors: the initial phase angle of the asteroid determines the angular position of the "bulge", while the shape of this oblong bulge is because of the sharp $\frac{1}{r^2}$ dependence of the forces. As the asteroid gets further away from the Sun, it no longer possesses enough kinetic energy to stay in a circular orbit of that given radius and falls inward to an eccentric orbit. This behavior will be explored more in the next subsection.

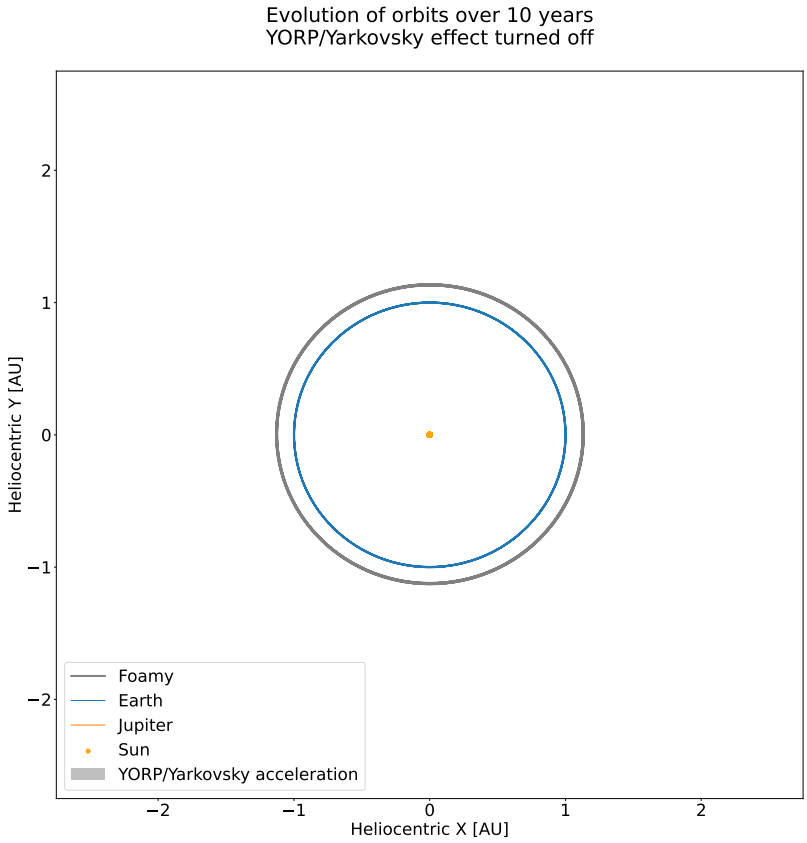

Figure 3: The evolution of the orbit of an asteroid with initial conditions as listed in Table 1, without YORP/Yarkovsky forces.

3.1 Orbital Parameters

The plot of the change in semi-major axis and eccentricity is visible in 4. Again, the effect of the Yarkovsky radial thrust is evident in the upward trend of the semi-major axis. Recall that the gravity of Jupiter has a large effect on asteroids in the Solar system; plots detailing the exact impact of Jupiter on our singular asteroid can be found in Figure 6 (Appendix 5). Allowing for this, with YORP and Yarkovsky turned off, the semi-major axis and eccentricity of the asteroid remain approximately constant.

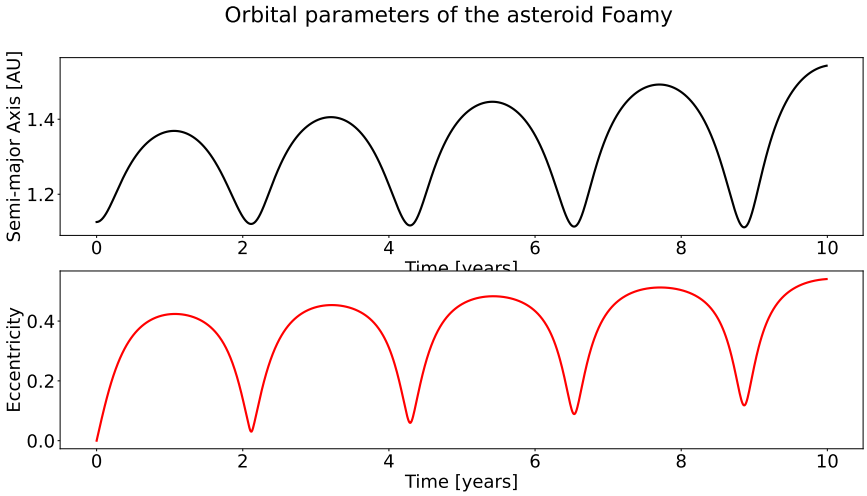

(a) YORP/Yarkovsky effect turned on.

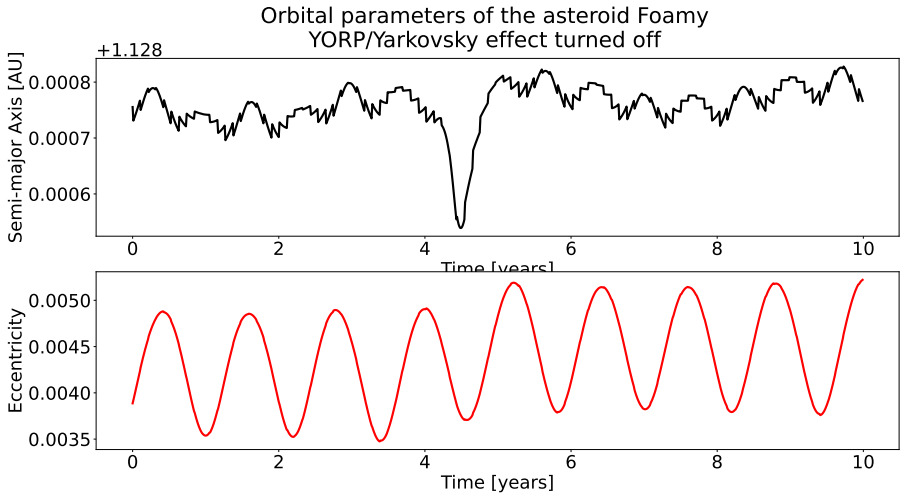

(b) YORP/Yarkovsky effect turned off. The jagged pattern can be attributed to the influence of Jupiter (see Figure 6).

Figure 4: The evolution of the semimajor axis and eccentricity of an asteroid with initial conditions as listed in Table 1.

3.2 Flux

The flux plot is displayed in 5. The characteristic peaks in the plot correspond to the moments when the asteroid and observer are in the closest proximity, and when they directly face each other (as all bodies in the simulation are point masses, occultation was not taken into account). Considering that at the aforementioned points the full face of the illuminated asteroid can be seen by the observer thus maximizing the flux, and that intensity has a $\frac{1}{r^2}$ dependence on distance, the results of the plot follow logically.

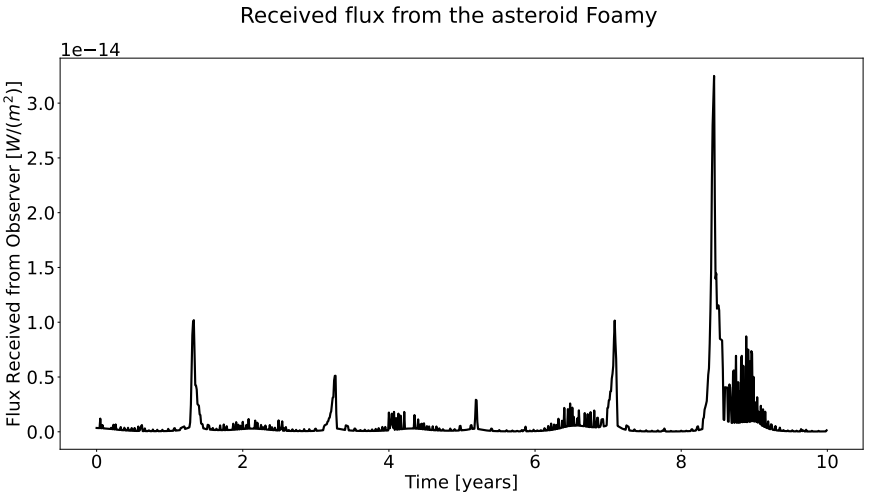

Figure 5: The flux received on Earth from an asteroid with initial conditions as listed in Table 1.

4 Discussion

4.1 Caveats and Uncertainties

In the process of simulation, simplifications were made that must be taken into account. As it stands, the simulation does not consider occultation, when light from the source would be blocked due to the eclipse of celestial bodies. If we were able to include occultation in our simulation, it would result in a distinct change in the flux plot. The flux would go to zero at the center of each large peak in the graph; this would indicate points where one

of the celestial bodies blocked the asteroid from view of the other. Ideally, occultation inclusion would also involve treatment of the Solar system bodies as non-point sources. However, treating the Sun as a non-point source would involve reverse ray-tracing, taking each ray of light that reached the observer and tracing it back to the asteroid, then to the light source. Reverse ray-tracing is computationally complex, and though it may be a more accurate way to simulate the desired light curves, it is beyond the scope of this project.

This work makes the assumption that all celestial bodies exist in the same orbital plane. As the Solar system is unusually flat in this regard, the assumption has a smaller impact than it would for a non-Solar system, but a three-dimensional simulation must be more accurate and useful for future progress.

An additional parameter that could be improved upon is the temperature. In the code, temperature is calculated using the flux incident on the asteroid. This implies that at any time when a patch on the asteroid is no longer receiving direct flux, its temperature instantly drops to zero, when in reality the patch radiates its heat over time, producing a tiny thrust all the while. This effect would contribute to a change in the asteroid's rotation as well as its orbital position, and would especially need to be adressed in the case of non-spherical asteroid simulation.

Finally, our results cannot of course be entirely accurate without the inclusion of the other Solar system planets, whose gravity must affect our singular asteroid. However, our objective in this work was to simulate a force which can be difficult to discern when contending with the gravitational effects of a multitude of celestial bodies. We therefore content ourselves with the inclusion of Jupiter, the greatest planetary perturber, and leave the full Solar system simulation to a future work.

4.2 Further Action

The scripts for this work were written with the intention of being generalizable, implying a vast potential for further action. The most evident modification would involve simulation of a large quantity of asteroids in order to derive results with relevant consequences in regards to effects on our Solar

system. A further generalization would entail initializing the asteroids with non-spherical shapes to examine how the YORP and Yarkovsky forces would affect their orbits and rotations. Beneficial in this setup would be implementation of an observationally accurate albedo, rather than the randomized patch setup utilized in this work.

The simulation variability stretches further to non-Solar systems; multiple-star systems, asteroid binaries, or different planets and resonances. Additional possibilities involve the tracking of non-asteroid objects, such as satellites or planetary remnants. As an example, evolution of the central star within the simulation would allow flexibility for the observation of planetary remnants around a white dwarf.

5 Conclusions

We have succeeded in the creation of a code that utilizes AMUSE framework in order to simulate the effects of a particular field code on asteroids in a Solar system similar to ours. Its results are directly relevant to events on Earth, as the simulation shows the possibility that the YORP/Yarkovsky effects could induce an asteroid to move within impact range of the Earth. The easily generalizable nature of the code allows for a greater level of accuracy when simulating our Solar system, as well as future ability to simulate asteroid sized objects in any bound system.

References

Conor J. Benson and Daniel J. Scheeres. Averaged Solar Torque Rotational Dynamics for Defunct Satellites. *Journal of Guidance Control Dynamics*, 44(4):749–766, April 2021. doi: 10.2514/1.G005449.

Joseph A. Burns and Douglas P. Hamilton. Debris About Asteroids: Where and How Much? In Alan W. Harris and Edward Bowell, editors, *Asteroids, Comets, Meteors 1991*, page 101, December 1992.

J. Durech, D. Vokrouhlický, M. Kaasalainen, et al. Detection of the YORP effect in asteroid (1620) Geographos. *A&A*, 489(2):L25–L28, October 2008. doi: 10.1051/0004-6361:200810672.

Carl Hergenrother, C. Maleszewski, Michael Nolan, et al. The operational environment and rotational acceleration of asteroid (101955) bennu from osiris-rex observations. *Nature Communications*, 10:1291, 03 2019. doi: 10.1038/s41467-019-09213-x.

M. Kaasalainen and J. Torppa. Optimization Methods for Asteroid Lightcurve Inversion. I. Shape Determination. *Icarus*, 153(1):24–36, September 2001. doi: 10.1006/icar.2001.6673.

M. Kaasalainen, J. Torppa, and K. Muinonen. Optimization Methods for Asteroid Lightcurve Inversion. II. The Complete Inverse Problem. *Icarus*, 153(1):37–51, September 2001. doi: 10.1006/icar.2001.6674.

Mikko Kaasalainen, Josef Ďurech, Brian D. Warner, et al. Acceleration of the rotation of asteroid 1862 Apollo by radiation torques. *Nature*, 446(7134): 420–422, March 2007. doi: 10.1038/nature05614.

S. C. Lowry, P. R. Weissman, S. R. Duddy, et al. The internal structure of asteroid (25143) Itokawa as revealed by detection of YORP spin-up. *A&A*, 562:A48, February 2014. doi: 10.1051/0004-6361/201322602.

Stephen C. Lowry, Alan Fitzsimmons, Petr Pravec, et al. Direct detection of the asteroidal yorp effect. *Science*, 316(5822):272–274, 2007. doi: 10.1126/science.1139040. URL `https://www.science.org/doi/abs/10.1126/science.1139040`.

Shantanu P. Naidu, Steven R. Chesley, Davide Farnocchia, et al. Anticipating the DART Impact: Orbit Estimation of Dimorphos Using a Simplified Model. *PSJ*, 3(10):234, October 2022. doi: 10.3847/PSJ/ac91c0.

Michael Nolan, Ellen Howell, D. Scheeres, et al. Detection of rotational acceleration of bennu using hst light curve observations. *Geophysical Research Letters*, 46, 02 2019. doi: 10.1029/2018GL080658.

A. Rossi, F. Marzari, and D. J. Scheeres. Computing the effects of YORP on the spin rate distribution of the NEO population. *Icarus*, 202(1):95–103, July 2009. doi: 10.1016/j.icarus.2009.02.030.

David Parry Rubincam. Radiative spin-up and spin-down of small asteroids. *Icarus*, 148(1):2–11, 2000. ISSN 0019-1035. doi: https://doi.org/10.1006/icar.2000.6485. URL `https://www.sciencedirect.com/science/article/pii/S0019103500964856`.

Patrick A. Taylor, Jean-Luc Margot, David Vokrouhlický, et al. Spin Rate of Asteroid (54509) 2000 PH5 Increasing Due to the YORP Effect. *Science*, 316(5822):274, April 2007. doi: 10.1126/science.1139038.

Jun Tian, Haibin Zhao, and Bin Li. Shape model and rotation acceleration of (1685) Toro and (85989) 1999 JD6 from optical observations. *arXiv e-prints*, art. arXiv:2209.13333, September 2022.

J. Ďurech, D. Vokrouhlický, A. R. Baransky, et al. Analysis of the rotation period of asteroids (1865) Cerberus, (2100) Ra-Shalom, and (3103) Eger - search for the YORP effect. *A&A*, 547:A10, November 2012. doi: 10.1051/0004-6361/201219396.

J. Ďurech, D. Vokrouhlický, P. Pravec, et al. YORP and Yarkovsky effects in asteroids (1685) Toro, (2100) Ra-Shalom, (3103) Eger, and (161989) Cacus. *A&A*, 609:A86, January 2018. doi: 10.1051/0004-6361/201731465.

J. Ďurech, D. Vokrouhlický, P. Pravec, et al. Rotation acceleration of asteroids (10115) 1992 SK, (1685) Toro, and (1620) Geographos due to the YORP effect. *A&A*, 657:A5, January 2022. doi: 10.1051/0004-6361/202141844.

Dimitri Veras, Yusuf Birader, and Uwais Zaman. Orbit decay of 2-100 au planetary remnants around white dwarfs with no gravitational assistance

from planets. *MNRAS*, 510(3):3379–3388, March 2022. doi: 10.1093/mnras/stab3490.

D. Vokrouhlický, W. F. Bottke, S. R. Chesley, et al. The Yarkovsky and YORP Effects. In *Asteroids IV*, pages 509–531. 2015. doi: 10.2458/azu_uapress_9780816532131-ch027.

Tarik J Zegmott, S C Lowry, A Rożek, et al. Detection of the YORP effect on the contact binary (68346) 2001 KZ66 from combined radar and optical observations. *Monthly Notices of the Royal Astronomical Society*, 507(4): 4914–4932, 09 2021. ISSN 0035-8711. doi: 10.1093/mnras/stab2476. URL `https://doi.org/10.1093/mnras/stab2476`.

J. Ďurech, D. Vokrouhlický, M. Kaasalainen, et al. New photometric observations of asteroids (1862) apollo and (25143) itokawa - an analysis of yorp effect. *Astronomy and Astrophysics*, 488:345–350, 09 2008. doi: 10.1051/0004-6361:200809663.

Appendix

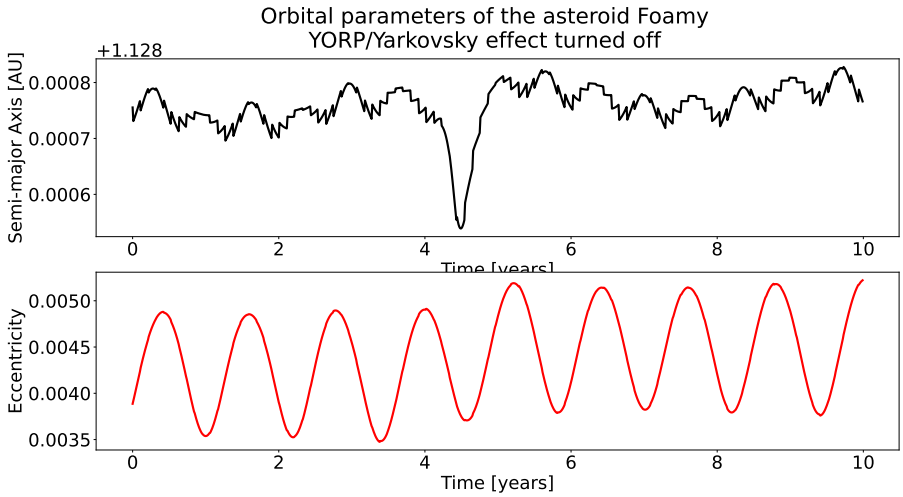

(a) Jupiter is present

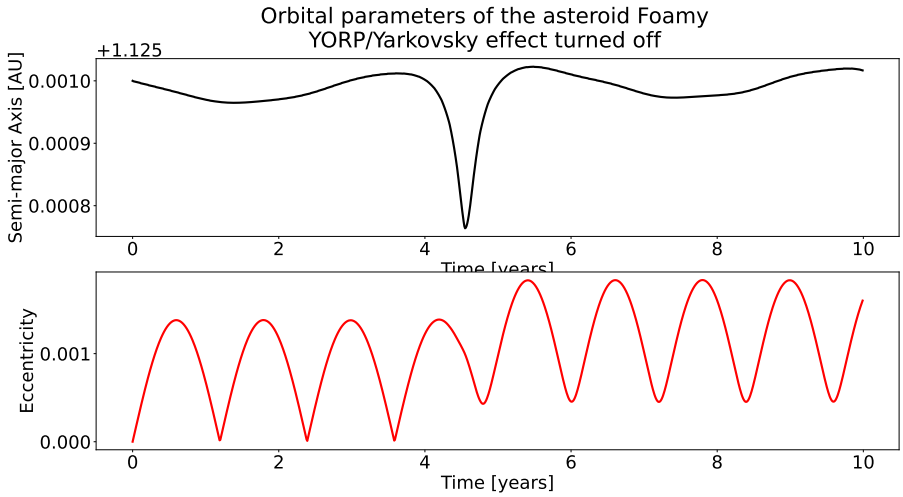

(b) Jupiter is not present

Figure 6: The effect of Jupiter on the evolution of the semimajor axis and eccentricity of an asteroid. Initial conditions as in Table 1, unless indicated otherwise.